

**IRAS FSC 15307+3252:  
Gravitationally Lensed Seyfert or Cannibal Elliptical at  $z = 0.93$ ?<sup>1</sup>**

Michael C. Liu and James R. Graham<sup>2</sup>

Department of Astronomy, University of California, Berkeley, CA 94720

email: [mliu, jrg]@astro.berkeley.edu

and

Gillian S. Wright

Joint Astronomy Centre, 660 N. A'ohōkū Place, University Park, Hilo, HI 96720

email: gsw@jach.hawaii.edu

To appear in the October 20, 1996 issue of the *Astrophysical Journal*

**ABSTRACT**

We present the highest spatial and spectral resolution near-infrared data to date of the  $\sim 10^{13} h^{-2} L_{\odot}$  IRAS source FSC 15307+3252 at  $z = 0.93$ , apparently the most luminous galaxy in the known Universe. Deep  $K$ -band ( $2.2 \mu\text{m}$ ) images taken in  $0''.4$  seeing at the W. M. Keck Telescope reveal three components: (A) a bright elliptical source with a compact nucleus, (B) a resolved circular companion separated from component A by  $2''.0$  ( $8h^{-1}$  kpc for  $q_0 = 0.5$ ), and (C) a faint irregular component  $1''.7$  from A. The surface brightness profile of F15307-A is well-characterized by a de Vaucouleurs  $r^{1/4}$  law with  $r_e = 1''.4 \pm 0''.2$  ( $6h^{-1}$  kpc), a size comparable to local giant ellipticals. The nucleus of component A is stellar in appearance with extended structure, possibly a second nucleus  $\sim 0''.5$  away. Our  $1.1\text{--}1.4 \mu\text{m}$  spectrum of the F15307 system with a resolution of  $330 \text{ km s}^{-1}$  shows strong emission lines of [O I]  $\lambda\lambda 6300, 6364$ ; blended  $\text{H}\alpha + [\text{N II}] \lambda\lambda 6548, 6583$ ; and [S II]  $\lambda\lambda 6716, 6731$ . The  $\sim 900 \text{ km s}^{-1}$  width of the forbidden lines and the relative strengths of the emission lines are characteristic of Seyfert 2 galaxies. The  $\text{H}\alpha$  line also has a broad ( $1900 \text{ km s}^{-1}$ ) component.

In light of the recent discovery that FSC 10214+4724, previously the most luminous known galaxy, is a gravitationally-lensed system, we explore the possibility that F15307 is also lensed. Quantitative arguments are inconclusive, but aspects of F15307's morphology do suggest lensing; the system bears a strong resemblance to

---

<sup>1</sup>Based in part on observations obtained at the W.M. Keck Observatory, which is operated jointly by the University of California and the California Institute of Technology.

<sup>2</sup>Alfred P. Sloan Fellow.

quadruple-image gravitational lenses. On the other hand, given the  $r^{1/4}$  profile, the close companions, and the active nucleus, F15307 may in fact be a giant elliptical galaxy caught in the act of galactic cannibalism, a scenario which could also account for its unparalleled luminosity.

*Subject headings:* cosmology: gravitational lensing — galaxies: formation — galaxies: individual (IRAS FSC 15307+3252) — galaxies: photometry — galaxies: starburst — infrared: galaxies

## 1. Introduction

During the course of an *IRAS* color-selected survey for extremely luminous IR-bright galaxies, Cutri et al. (1994) identified FSC 15307+3252 as an  $\sim 1.0 \times 10^{13} h^{-2} L_{\odot}$  galaxy at a redshift of 0.926 ( $q_0 = 0.5$ ,  $H_0 = 100h \text{ km s}^{-1} \text{ Mpc}^{-1}$ ). They found its restframe UV/blue optical spectrum resembles a Seyfert 2 galaxy; Soifer et al. (1994) found a similar result for the restframe red optical emission lines though they had insufficient spectral resolution to measure linewidths. Hines et al. (1995) have found broad Mg II  $\lambda 2798$  emission and a power-law continuum in polarized light, leading them to argue the system contains a buried quasar. IR imaging by Soifer et al. (1994) in  $1''$  seeing shows the system is composed of a bright extended source with one or two close companions.

The one known galaxy believed to be more luminous than F15307, the  $\sim 5 \times 10^{13} h^{-2} L_{\odot}$  source FSC 10214+4724 at  $z = 2.286$ , is now known to be the first example of a gravitationally-lensed Seyfert 2 galaxy. Its *I*-band flux is magnified by a factor of 100 (Eisenhardt et al. 1996), and the *K*-band magnification is around 10–20 (Graham & Liu 1995, Broadhurst & Lehár 1995). In hindsight, this result is not surprising. Many known lensed systems are  $z \gtrsim 1$  quasars. In the local universe, the space density of luminous ( $L \gtrsim 10^{11} L_{\odot}$ ) IR galaxies exceeds that of quasars (Soifer et al. 1986); if this fact holds at higher redshifts, one naturally expects gravitational lensing of IR-bright galaxies. *IRAS* sources at  $z \gtrsim 0.5$  are prime suspects for this phenomenon since the associated magnification would allow these objects to be detected at significant redshifts. Statistical estimates support this line of reasoning (Broadhurst & Lehár 1995, Trentham 1995). However, while lensed quasars are relatively easy to identify since lensing of point sources produces distinctive sets of multiple images, lensed extended sources, like IR-bright galaxies, are more difficult to recognize for two reasons: (1) their total magnification is less, and (2) they form extended images which require high angular resolution to resolve, e.g., sub-arcsecond interferometric imaging is needed to identify lensed high redshift radio lobes (e.g., Blandford & Narayan 1992).

Therefore, high resolution imaging of F15307 is necessary in order to determine whether its extraordinary luminosity arises from gravitational lensing or intrinsic phenomena such as massive

starbursts and/or an active nucleus. If F15307 and other high- $z$  *IRAS* sources are gravitationally lensed like F10214, this discovery will have applications beyond understanding the nature of these objects. Lensed extended sources are useful tools for probing the mass distribution of the lensing galaxies since they offer more lines of sight through the lens than lensed point sources (e.g., Kochanek 1991). Imaging provides a more effective tool to search for lensing than spectroscopy, since the latter typically requires high S/N to search for discrepant redshifts from continuum features. Targets found with morphologies suggestive of lensing can then be spectroscopically examined to determine a redshift for the foreground lens. Ultimately, statistics of these lensed systems will quantify the magnification bias afflicting the high end of the *IRAS* luminosity function.

In this paper we present  $0''.4$  resolution  $K$ -band imaging and moderate resolution ( $\lambda/\Delta\lambda = 990$ ) near-IR (1.1–1.4  $\mu\text{m}$ ) spectroscopy of FSC 15307+3252. Our imaging data identify three components all within  $2''$ . The near-IR (restframe optical) spectrum displays emission lines of [O I],  $\text{H}\alpha + [\text{N II}]$ , and [S II] which resemble a Seyfert 2-type spectrum. The morphology of the system is similar to quadruple-image gravitational lenses, though at the limit of our resolution, we cannot discount the possibility the system is involved in a close interaction and/or merger of 2–3 separate components; in particular, the brightest component appears to be a large elliptical galaxy in the process of assembling. Throughout the paper we assume  $q_0 = 0.5$  and  $H_0 = 100h$   $\text{km s}^{-1} \text{Mpc}^{-1}$ . With this choice of cosmology,  $1''$  corresponds to  $4.2h^{-1}$  kpc at a redshift of 0.926.

## 2. Observations and Data Reduction

### 2.1. Imaging

We observed F15307 on 1995 May 23 (UT) using the facility near-IR camera (Matthews & Soifer 1994) of the 10-meter W. M. Keck Telescope located on Mauna Kea, Hawaii. The camera employs a Santa Barbara Research Corporation  $256 \times 256$  InSb array and has a plate scale of  $0''.15 \text{ pixel}^{-1}$ . We observed using the standard  $K$  (2.0–2.4  $\mu\text{m}$ ) filter. We used an integration time of 10 s per coadd, and after six or ten frames were coadded and saved as an image, we offset the telescope by a few arcseconds. The telescope was stepped using a non-redundant dither pattern. An off-axis CCD camera was used to guide the telescope during the observations. The total integration time was 2100 s.

We constructed a flat field by median averaging the images after subtraction of a dark frame to remove the bias level; a preliminary sky subtraction was performed to identify astronomical objects so as to exclude them from the averaging. Then for each frame, we subtracted a local sky frame constructed from the average of prior and subsequent frames, again excluding any astronomical objects from the averaging. We used the bright star  $\approx 20''$  north of F15307 to register the reduced frames and then shifted by integer pixel offsets to assemble a mosaic of the

field. Bad pixels were identified and masked during the construction of the mosaic; we avoided interpolating pixel values. We performed all the reductions and analysis using Research System Incorporated’s IDL software package (version 4.0.1) unless otherwise noted.

We observed the faint UKIRT standard FS 27 ( $K = 13.123 \pm 0.018$ ; Casali & Hawarden 1992) immediately before F15307 as a flux calibrator. Our derived zero point, the magnitude of a star which produces 1 count for a 1 second integration, is  $25.22 \pm 0.02$  mag. The sky was moonless so it was difficult to determine at the time if it was clear. Photometry of the aforementioned bright star in the individual frames had a standard deviation of 5% with a slight trend toward fewer counts during the course of the observations. We measure a  $K$  magnitude for this star 0.08 mag fainter than Soifer et al. (1994), and taking this offset into account, our photometry for F15307 in 6''–9'' diameter apertures is consistent with theirs. Throughout the paper we use our derived photometry as any systematic errors are of order 5% or less.

Figure 1 shows our final  $K$ -band mosaic. The central  $25'' \times 25''$  region achieves  $1 \sigma$  noise of  $23.9 \text{ mag arcsec}^{-2}$ . The faintest objects in the image are  $K \approx 21.5 - 22$  mag. The spatial resolution of the mosaic, as determined from the full width at half maximum (FWHM) of the brightest star in the field, is  $0''.4$ . For brevity, we will refer to this star as the “bright star” (called “star A” by Soifer et al. 1994). Nearly all other objects in the mosaic are extended.

Table 1 presents relative astrometry and photometry for objects in the field identified by eye. With the exception of F15307, the photometry is measured in a 3'' diameter aperture using a 6''–9'' diameter annulus for sky level determination and adjusted by a small (0.03 mag) aperture correction derived from the bright star. The components of F15307 were measured in 2'' (component A), 1''.5 (B), and 1'' (C) diameter apertures modified by the appropriate aperture corrections; as we discuss in § 3.2, the expected contamination from  $K$ -band line emission is negligible. Photometry errors were calculated by combining in quadrature the noise in the photometry aperture with errors in the zero point and sky level determination. The number and brightnesses of the objects in the F15307 field are consistent with  $K$ -band galaxy number counts (Gardner et al. 1993, Djorgovski et al. 1995). Note that using the calculations from § 4.1, components A and B have  $K$  magnitudes equivalent to  $\sim 5$  and 1  $L^*$  ellipticals at  $z = 0.926$ , respectively.

## 2.2. Spectroscopy

We obtained a  $J$ -band spectrum of F15307 on 1995 July 13 (UT) using the facility long slit spectrograph CGS4 (Mountain et al. 1990) of the United Kingdom Infrared Telescope (UKIRT) located on Mauna Kea, Hawaii.<sup>3</sup> We employed the 75 lines  $\text{mm}^{-1}$  grating in second order to

---

<sup>3</sup>UKIRT is operated by the Royal Observatory, Edinburgh, on behalf of the UK Science and Engineering Research Council.

obtain a nominal resolution ( $\lambda/\Delta\lambda$ ) of 990 ( $330 \text{ km s}^{-1}$ ) with  $0.33 \mu\text{m}$  wavelength coverage, and we oriented the slit to within  $1^\circ$  of north-south. Conditions were photometric. The spectrograph camera images one pixel across the  $1''.5$  slit so in order to fully sample the instrument profile the detector was stepped  $1/2$  pixel in the spectral direction after a 30 second on-chip exposure time. The source was nodded between two positions on the slit every minute, after each fully sampled spectrum was obtained. The observation consisted of 20 such nodded pairs for total time exposure of 40 minutes. Observations of the blackbody and krypton lamp in the CGS4 calibration unit were obtained for flat field and wavelength calibration. The nearby G3V star HR 5728 was observed with the same nodding technique before and after observing F15307 as an atmospheric standard, and a spectrum of HD 136754 (Elias et al. 1982) was obtained for flux calibration.

Data reduction was carried out using the Figaro data reduction package (Shortridge 1993). Each individual spectrum was flat fielded, the nodded data subtracted in pairs, and the pairs coadded. Wavelength calibration from the krypton lamp was accurate to  $0.0005 \mu\text{m}$ , as determined by our measurement of Paschen  $\beta$  absorption in HD 136754 at  $1.2827 \mu\text{m}$ . We used the method of Horne (1986) to extract the spectra from the two slit positions and then summed the extractions. The spectra of the two standard stars were reduced and extracted in the same fashion as the galaxy spectrum. Atmospheric absorption in the spectrum of F15307 was corrected by using the spectrum of HR 5728, which was corrected to the same mean airmass and divided by a  $5770 \text{ K}$  blackbody. Flux calibration was derived from the spectrum of HD 136754, assuming a  $J$  magnitude of 7.135.

Figure 2 presents our reduced spectrum. The spectrum of the F15307 system possesses emission lines of [O I]  $\lambda\lambda 6300, 6364$ ;  $\text{H}\alpha + [\text{N II}] \lambda\lambda 6548, 6583$ ; and [S II]  $\lambda\lambda 6716, 6731$ . The possible narrow feature at  $1.165 \mu\text{m}$  lies  $\sim 3000 \text{ km s}^{-1}$  blueward of the expected position of [Fe VII]  $\lambda 6087$ ; curiously, the very broad ( $\sim 10^4 \text{ km s}^{-1}$ ) polarized Mg II  $\lambda 2798$  line detected by Hines et al. (1995) is blueshifted this same amount from the unpolarized narrow Mg II component. If the [Fe VII] identification is correct the feature is unusually strong compared to other narrow-lined AGN (Osterbrock 1989), but this line can be strong in highly photoionized regions such as the radio galaxy PKS 2152–69 (Tadhunter et al. 1988).

### 3. Data Analysis and Results

#### 3.1. *K*-band Morphology

Figure 3 shows the structure of F15307 and the designations we will use for the three prominent components. The brightest source, component A, is elliptical with a position angle (PA) of  $\approx 40^\circ$  and a major to minor axis ratio of  $\approx 1.2$ . The PA is the angle between north and the major axis of component A, measured east from north. Component B, the next brightest source, lies  $2.0''$  ( $8h^{-1} \text{ kpc}$ ) to the southeast of component A. It is resolved into an extended source and is roughly circular. The faintest source, component C, is  $1''.7$  east of component A and

far more irregular in appearance than the other two sources. Low-level diffuse emission surrounds the entire system, with a total extent of about  $6''$  ( $25h^{-1}$  kpc) and roughly an elliptical shape with a different PA than component A. Based on  $K$  band number counts, it is unlikely the three components are a chance superposition of objects at different redshifts (Soifer et al. 1994).

### 3.1.1. F15307-A: An Elliptical Galaxy with Nuclear Structure

Given the excellent angular resolution of the image, we are able to study quantitatively the morphology of component A. We extracted the surface brightness (SB) profile of this component using elliptical apertures with the aforementioned PA and axial ratio spaced by the seeing FWHM. A  $6''$ – $9''$  radius elliptical annulus was used to determine the sky level. We included pixels only from the northwestern half of F15307-A (PA from  $215^\circ$  to  $35^\circ$ ) to avoid contamination from the other two components and computed errors by summing in quadrature the standard error in each annulus with the (essentially negligible) sky error determined from the scatter in the sky annulus pixels. We then fitted the profile from  $1''$ – $3''$  in semi-major axis with de Vaucouleurs  $r^{1/4}$  and exponential disk profiles (e.g., Mihalas & Binney 1981) using a standard non-linear least-squares algorithm; we avoided the central  $1''$  to reduce seeing effects and contamination by any unresolved nuclear component. The de Vaucouleurs profile provided a very good fit while the exponential profile did not, as judged both by eye and by the reduced chi-square values ( $\tilde{\chi}^2 = 0.4$  versus 4.7). The isophotes of component A rotate slightly over the fitting range, but this fact should not strongly affect the fitting. Figure 4 displays component A’s SB profile along with the de Vaucouleurs and exponential fits.

To quantify systematic effects from seeing, we repeated the fitting process on artificial models of galaxies with de Vaucouleurs and exponential profiles over a range of SBs and scale lengths. We convolved the artificial galaxies with the bright star as a representation of the point spread function (PSF), subpixelating the model and psf before convolution and rebinning afterwards. We then added Gaussian noise equal to the amount in the reduced image of F15307 and applied the fitting algorithm to the artificial galaxies. For a given model galaxy, we added noise and performed the fit many times. Our tests confirm we can effectively distinguish between de Vaucouleurs and exponential models over the relevant range of parameters and that the formal statistical errors derived from the fit are reasonable. Our tests also suggest we have systematically underestimated  $\mu_e$  by  $\simeq 0.5$  mag arcsec $^{-2}$  and  $r_e$  by  $\simeq 20\%$ . For F15307-A we derive final values for the  $K$ -band de Vaucouleurs profile of  $\mu_e = 20.1 \pm 0.3$  mag arcsec $^{-2}$  and  $r_e = 1''.4 \pm 0''.2$  ( $6h^{-1}$  kpc).

Figure 5 shows our image of F15307 after subtraction of a seeing-convolved de Vaucouleurs profile juxtaposed against the PSF. The residuals show a bright compact source at the center F15307-A with a sub-arcsecond extension to the southwest (PA  $\sim 220^\circ$ ). The flux in a  $1''.5$  diameter aperture centered on the core is 17.6 mag, about 1/3 of the total flux in this region. This source likely does not significantly contaminate our de Vaucouleurs fits; applying our SB fitting procedure on the PSF shows the PSF wings have a much smaller scale length than component A.

Our analysis in § 3.1.2 verifies the reality of this nuclear structure and hints that the extension seen in the residual image is a second compact source  $\sim 0''.5$  ( $2h^{-1}$  kpc) from the central nucleus and  $\sim 10$  times fainter. This structure is also present in images deconvolved with the Lucy-Richardson algorithm (Lucy 1974, Richardson 1972) as implemented in IRAF (version 2.10.3).<sup>4</sup>

### 3.1.2. The Companions: F15307-B and F15307-C

To study components B and C better, we removed the emission associated with component A assuming elliptical symmetry. In addition to subtracting a de Vaucouleurs profile (§ 3.1.1), we removed component A using two other methods: (1) by subtracting its SB profile directly from the image and (2) by subtracting a  $180^\circ$  rotated version of the NW half from the SE half. All methods produced comparable results to the image shown in Figure 5. The relative astrometry of the three components in Table 1 uses the averages of measurements taken from the subtracted image and the original image. The error in the relative positions of A and B is  $\sim 0''.02$  and between A and C is  $\sim 0''.04$  based on the results from the different methods.

Component B is circular and clearly extended with a FWHM of  $0''.5$ . Its  $K$  magnitudes in  $1''.5$  and  $2''.5$  diameter apertures with a point source-derived aperture correction are  $18.6 \pm 0.1$  and  $18.2 \pm 0.1$ , respectively. There is faint emission along the axis connecting A and B.

Component C is noticeably more diffuse than either A or B. It may not be a distinct component at all but rather a tidal feature, though it would then have to be intrinsically bright to overcome cosmological surface brightness dimming. Its inner ( $\sim 0''.5$  diameter) isophotes are extended roughly north-south while the  $\sim 1''$  diameter isophotes are approximately perpendicular to the axis connecting A and B and extended preferentially to the NE. Aperture-corrected photometry in a  $1''$  diameter aperture gives  $K \approx 20.1 \pm 0.1$  mag.

## 3.2. Emission Line Spectrum

We measured each set of close lines ([O I],  $H\alpha$  + [N II], [S II]) independently, approximating each line as a Gaussian. FWHMs for the lines of each doublet were constrained to be the same, and the FWHM was allowed to vary between doublets. The line ratios of the [O I] and [N II] doublets were fixed. We varied the [S II] line ratio from the low to high density limit; the high density limit fit slightly better though it produced a greater redshift discrepancy between [O I] and [S II]. Our measured [O I] and [S II] FWHMs are  $900 \pm 300$  km s<sup>-1</sup> and  $900 \pm 600$  km s<sup>-1</sup>, respectively, comparable to those of the restframe blue/UV forbidden lines (Cutri et al. 1994).

---

<sup>4</sup>IRAF (Image Reduction and Analysis Facility) is distributed by the National Optical Astronomy Observatories, which are operated by the Association of Universities for Research in Astronomy, Inc., under cooperative agreement with the National Science Foundation.

We deblended  $H\alpha + [N II]$  with three methods. First, we constrained the  $[N II]$  linewidths to be the same as  $[O I]$  and  $[S II]$ ;  $[N II]$  has a critical density in between the two so this assumption is reasonable (Filippenko & Halpern 1984, Filippenko 1985, De Robertis & Osterbrock 1986). In the second method, both the  $H\alpha$  and  $[N II]$  linewidths were allowed to vary. In the third method, we constrained the FWHM of  $[N II]$  and  $H\alpha$  to be the same as  $[O I]$  and  $[S II]$  and added a broad component of  $H\alpha$ , attempting to account for narrow  $H\alpha$  emission from starbursts and HII regions and broader emission from an AGN. In all the methods, the redshifts of the  $H\alpha$  and  $[N II]$  lines were free parameters. All methods find comparable redshifts, FWHMs, and equivalent widths for the lines as well as a significant broad ( $1910 \pm 50 \text{ km s}^{-1}$  FWHM) component to the  $H\alpha$  line. We conservatively constrain any very broad  $H\alpha$  component to have a restframe equivalent width  $\lesssim 0.10 \mu\text{m}$ , assuming it has the same  $\sim 10^4 \text{ km s}^{-1}$  FWHM as the polarized broad  $Mg II \lambda 2798$  line (Hines et al. 1995).

Table 2 provides the extracted physical parameters. The errors are from the formal fitting errors. We list results from the high-density fit to  $[S II]$  and the deblending of  $H\alpha + [N II]$  which incorporates a narrow and broad  $H\alpha$  component. The total observed equivalent width of the lines is  $0.10 \pm 0.01 \mu\text{m}$ , which accounts for  $\approx 40\%$  of the spectrum’s  $J$ -band flux. Using the  $H\alpha$  flux, we can predict the emission line contamination to the  $K$ -band observations is negligible. The strongest relevant line is  $He I \lambda 10830$  (Rudy et al. 1989, Osterbrock et al. 1990, Rudy et al. 1993). Using typical flux ratios of  $He I$  to  $H\alpha$  observed by Rudy et al. (1989) in Seyfert 2 galaxies, the  $K$ -band line contamination to the integrated F15307 flux is expected to be  $\lesssim 5\%$  and  $\lesssim 10\%$  if we consider only the inner  $2''$  of F15307-A and assume it is the lone source of line emission.

A variety of diagnostics show the spectrum is Seyfert 2-type. The FWHM of the lines is consistent with such a spectrum, though both the permitted and forbidden linewidths are somewhat greater than typical of Seyfert 2’s (Osterbrock 1989, Osterbrock 1991). We also classified the spectrum using the excitation diagrams of Veilleux & Osterbrock (1987), supplemented with data from Ho, Filippenko, & Sargent (1993). We took the  $[O III] \lambda 5007$  flux from Soifer et al. (1994) and assumed  $H\alpha/H\beta = 2.9$ , appropriate for pure recombination with  $T = 10^4 \text{ K}$  (Osterbrock 1989). The location of F15307 in these diagrams is consistent with Seyfert 2 excitation. Though much of the width of the forbidden lines might be due to  $\sim 300 \text{ km s}^{-1}$  relative orbital motion between two of the components encompassed in our slit, such an aperture effect should not affect the Seyfert 2 classification from the excitation diagrams (Ho, Shields, & Filippenko 1993) nor the presence of the broad  $H\alpha$  component.

Our restframe equivalent widths for  $[O I]$  are larger and  $H\alpha + [N II]$  and  $[S II]$  are smaller than Soifer et al. (1994). Since our slit was  $1''.5$  and theirs was  $0''.6$ , the differences may indicate that the  $[O I]$  emission region is considerably extended compared to the source(s) of the other lines. Local luminous *IRAS* galaxies do show extended line emission with excitation gradients (Armus et al. 1990, Fehmers et al. 1994, Veilleux et al. 1995).

## 4. Discussion

### 4.1. An Example of Gravitational Lensing?

In light of the discovery that F10214 is a gravitationally lensed system, it is natural to ask if the apparent extraordinary luminosity of F15307 is also due to lensing. We can use the morphological information in our high angular resolution data to explore the lensing scenario in a quantitative fashion. To review § 3.1, F15307 can be decomposed into three components: (A) a large elliptical source with a bright star-like core and elongated nuclear structure; (B) a resolved circular companion separated  $2''.0$  from A; and (C) a diffuse irregular companion  $\sim 1''.7$  from A. The most plausible feature which could be ascribed to gravitational lensing is the nuclear structure of component A. The bright nucleus and close extension or second nucleus could be due to multiple imaging/stretching of a  $z = 0.93$  source by a foreground lens.

A natural suspect for the foreground lens is component B because the nuclear structure of A would then be tangential image stretching. To examine this hypothesis, we can calculate the expected angular separation between the lens and images based on an estimated lens mass as a function of assumed redshift. The Einstein ring radius for an isothermal sphere with a one-dimensional velocity dispersion  $\sigma$  is

$$\theta_E = 1''.40 \left( \frac{\sigma}{220 \text{ km s}^{-1}} \right)^2 \frac{D_{LS}}{D_{OS}}$$

where  $D$  is the angular diameter distance from lens to source (LS) and observer to source (OS), respectively (Blandford & Narayan 1992). To estimate  $\sigma$  for F15307-B, we start with its  $K$  magnitude in a  $2''.5$  diameter aperture (§ 3.1.2) and apply a small correction from Frogel et al. (1978) to adjust to an aperture of  $D_0$ , assuming B is an elliptical with  $D_0 = 30h^{-1}$  kpc. We take  $K$ -corrections from unevolving elliptical galaxy spectral templates of Bruzual & Charlot (1993) and choose  $M_B^* = -21.3$  mag (Efstathiou et al. 1988) to determine the luminosity of B. We then use the Faber-Jackson relation,  $L \sim (\sigma_{\parallel})^4$ , to convert the luminosity to line-of-sight stellar velocity dispersion  $\sigma_{\parallel}$ , with an  $L^*$  elliptical having  $\sigma_{\parallel} = 220 \text{ km s}^{-1}$  (Faber & Jackson 1976), and following Turner et al. (1984) and Gott (1977), we assign  $\sigma = \sqrt{1.5} \sigma_{\parallel}$ . In choosing  $z_{lens}$ , there is a trade-off between placing the lens closer or farther from us. Increasing  $z_{lens}$  means the inferred luminosity of B and, consequently,  $\sigma$  will increase; however,  $D_{LS}$  will fall. Conversely, moving the lens to lower redshifts increases  $D_{LS}$  but decreases the inferred luminosity and  $\sigma$  and consequently  $\theta_E$ . For  $z_{source} = 0.93$ , the maximum of  $\theta_E$  versus  $z_{lens}$  is shallow, with  $(\theta_E)_{max} = 0''.56$  at  $z_{lens} \approx 0.35$ . At this redshift, component B is 2 magnitudes fainter than  $L^*$ . Note the aperture correction and the choice of  $M_B^*$  do not strongly affect the calculation since  $\theta_E \sim L^{1/2}$  through the Faber-Jackson relation.

The predicted Einstein ring radius is nearly a factor of 4 smaller than the observed separation between the assumed lensing galaxy (component B) and resulting images (the nuclear structure of A); equivalently, the mass-to-light ratio we infer for B is 4 times larger than typical ellipticals.

However, this lensing scenario remains plausible. The gravitational potential of B may be elliptical in which case images will be formed inside and outside the Einstein radius (e.g., Grossman & Narayan 1988). The potential could be elliptical even though its  $K$ -band appearance is circular; a similar situation occurs in the case of F10214 (Broadhurst & Lehár 1995, Eisenhardt et al. 1996). In addition, the intrinsic  $\sim 25\%$  scatter in  $\sigma$  from the Faber-Jackson relation (Djorgovski & Davis 1987) could lead to a  $\sim 50\%$  increase in  $\theta_E$ , and mass distributions more sharply peaked than the isothermal sphere will also boost the expected separation. Extinction is an unlikely explanation since components A and B have comparable  $JHK$  colors (Soifer et al. 1994), and the amount of dust needed to make  $\theta_E = 2''$  would be enormous ( $A_V \approx 18$ ).

F15307 bears a strong resemblance to probable quadruple-image gravitational lens systems, e.g., PG 1115+080 (Kristian et al. 1993, Young et al. 1981, Weymann et al. 1980), MG 2016+112 (Lawrence et al. 1984, Garrett et al. 1994, Schneider et al. 1986), and especially MG J0414+0534 (Angonin-Willaime et al. 1994, Annis & Luppino 1993, Hewitt et al. 1992). Therefore, an alternative lensing scenario is one where components B and C and the nuclear structure of A are all produced by lensing, with the lensing galaxy producing the diffuse emission which lies inside and around these sources. If the  $z = 0.93$  source lies just inside of the fold of the lensing potential’s diamond caustic (e.g., Figure 6c and 6d of Blandford & Narayan 1992), four images will be produced with a configuration similar to the arrangement of B, C, and the nuclei of A. The source would need to be extended to explain the extended central structure of A and the resolved nature of B. One objection to this scenario is that none of the components, especially component A, appear tangentially stretched, though such an effect probably requires a factor of  $\sim 2$  better spatial resolution to discount completely. Moreover, the lensing galaxy must be considerably underluminous. For instance if the lensing galaxy is located at the most probable location,  $D_{OS} = 2D_{LS}$  in a flat universe (Peebles 1993, Gott et al. 1989) which corresponds to  $z_{lens} = 0.4$ , an  $L_*$  elliptical has  $K \approx 16$  mag and  $r_e \approx 2''$  ( $6h^{-1}$  kpc at  $z = 0.4$ ). Such a galaxy might account for the  $\sim 6''$  diffuse emission around F15307; however, the central region of such a galaxy would be apparent in our images so if the F15307 is a four-image lens, the lensing galaxy is likely underluminous for its mass.

Note that our identification of F15307-A as an elliptical galaxy (§ 3.1.1) is incompatible with most lensing scenarios. The galaxy shows no sign of distortion from elliptical symmetry which would occur if it was a lensed source at  $z = 0.93$ , and the apparent coincidence of the galaxy with the presumed lensed images (the nuclear structure of A) rules out the galaxy being the foreground lens since lensed images coinciding with their lenses are strongly demagnified (e.g., Blandford & Narayan 1992). If in fact F15307 is a lensed system, F15307-A is probably composed of one or two tangentially stretched images with diffuse emission from the foreground lensing galaxy, leading us to misidentify the outer  $1''$ - $3''$  emission as being centered on the nuclear structure. One final important point: even if the system is lensed, the fact that the components are extended means that, just like FSC 10214, the total magnification cannot be enormous; the system must be an intrinsically luminous galaxy.

#### 4.2. Or a Cannibal Elliptical at $z = 0.93$ ?

Alternatively, F15307 may be intrinsically the most luminous galaxy in the known Universe. Its physical characteristics and environment are consistent with the idea that F15307 is a higher redshift and more luminous analogue of the most luminous galaxies in the local universe, the ultraluminous ( $L_{IR} \gtrsim 10^{12} L_{\odot}$ ) *IRAS* galaxies (Sanders et al. 1988a). Most ultraluminous IR galaxies (ULIRGs) possess disturbed morphologies and two or more close companions (Sanders et al. 1988a, Sanders et al. 1988b, Armus et al. 1990, Melnick & Mirabel 1990, Leech et al. 1994, Clowes et al. 1995); a large fraction also possess close double nuclei with  $\lesssim 1$  kpc separations (Graham et al. 1990, Carico et al. 1990, Majewski et al. 1993, Armus et al. 1994). Evidence for interactions in these systems seems to correlate with their total luminosity as well as the presence of an active nucleus (Sanders et al. 1988a, Sanders 1992). Indeed the merging process is believed to play a central role in the ULIRG phenomenon, though the issue of whether the high far-IR luminosity arises from dust-enshrouded active nuclei and/or compact starburst remains controversial (e.g., Sanders et al. 1988a, Condon et al. 1991, Kormendy & Sanders 1992). Similar processes could energize the extraordinary far-IR luminosity and active nucleus in F15307.

There exist some similarities between F15307 and radio galaxies. Its  $K$  magnitude is comparable to  $z \approx 1$  radio galaxies, and its  $R - K$  and  $B - R$  colors (Cutri et al. 1994) compared to its  $K$  magnitude lie between radio galaxies and radio quasars (Dunlop et al. 1989). Also, F15307's radio power is considerable; assuming a power-law spectrum,  $L_{\nu} \sim \nu^{-\alpha}$ , the observed 8.2 GHz flux density (Cutri et al. 1994) extrapolates to a restframe 1.49 GHz flux density of  $6.0 \times 10^{23} h^{-2} \text{ W Hz}^{-1}$  and  $6.5 \times 10^{24} h^{-2} \text{ W Hz}^{-1}$  for  $\alpha = 0$  and 1, respectively. Using a canonical  $\alpha \sim 0.7$ , F15307 would be classified as radio-loud ( $L_{1.49\text{GHz}} > 2.5 \times 10^{24} h^{-2} \text{ W Hz}^{-1}$  [Woltjer 1990]), with its radio power exceeding that of typical ultraluminous *IRAS* galaxies by a factor of 10 (Condon et al. 1991) and the most radio-luminous ordinary galaxies by a factor of 100 (Condon 1990).

Circumstantial evidence argues that the dust in F15307 is not widespread. Our upper limit on very broad  $\text{H}\alpha$  emission (§ 3.2) implies  $(\text{H}\alpha/\text{Mg II}) \lesssim 35$  for the broad lines. Using the expected ratio for a unreddened quasar spectrum (Osterbrock 1989) and an ordinary interstellar extinction law (Mathis 1990), our data imply  $A_V \lesssim 3$  along the line of sight to the region scattering light from the broad-line region. Also, the ratio of the  $\text{H}\alpha$  line to the  $\text{H}\delta$  line (Hines et al. 1995) does not differ much from the value expected for pure recombination. Finally, the fact that the  $R - K$  color is quite blue compared to typical ellipticals (see below) suggests dust is not widespread. The dust which generates the large far-IR luminosity may have a compact spatial distribution.

Since its surface brightness profile is well-described by a de Vaucouleurs law, our data suggest F15307-A is an elliptical galaxy. The measured  $K$ -band (restframe  $J$ -band) SB profile should be a good tracer of F15307-A's dynamical structure since galaxian  $J$ -band emission arises from old mass-tracing stellar populations, although contributions from recent star formation are not entirely negligible (Bruzual & Charlot 1993), and is relatively insensitive to extinction. The properties derived from the SB profile (§ 3.1.1) are in accord with the identification of F15307-A

as an elliptical galaxy. The  $6h^{-1}$  kpc half-light radius of F15307-A lies in the upper range seen in local giant elliptical galaxies (Pahre et al. 1995, Sandage & Perelmuter 1990). Based on the calculations in § 4.1, a non-evolving elliptical at  $z = 0.93$  has  $R - K \approx 6$  mag; using our  $K$ -band measurement alone would suggest F15307-A has a restframe  $B$ -band  $\mu_e \approx 23$  mag arcsec $^{-1}$ , a value which is also in the range of local giant ellipticals (Sandage & Perelmuter 1990). However, the integrated light of F15307 has  $R - K \approx 3$  mag (Cutri et al. 1994), much bluer than a typical elliptical, which may signal on-going star formation in one or more of the components.

The fact that F15307 has more than two components leaves our interpretation of the physical situation ambiguous. Mergers of two disk galaxies is believed to result in an elliptical (Barnes & Hernquist 1992 and references therein). This phenomenon is seen in numerical simulations of galaxy collisions (e.g., Toomre & Toomre 1972, Barnes 1992) and in reality: optical and IR imaging have found  $r^{1/4}$  profiles in the centers of advanced disk-disk mergers (Schweizer 1982, Wright et al. 1990, Stanford & Bushouse 1991), and velocity dispersion measurements argue that merging systems will evolve into ellipticals (Lake & Dressler 1986, Doyon et al. 1994). Based on its SB profile, F15307-A is clearly an elliptical galaxy, but if we are observing its formation via disk-disk merger how do we account for the other companions? Multiple merger events are suspected to be responsible for the formation of cD ellipticals (e.g., Hausman & Ostriker 1978), which do show multiple nuclei (e.g., Matthews et al. 1964); however, cD’s are exclusively found in clusters (Beers & Geller 1983, Morgan et al. 1975), and no cluster is known to be associated with F15307.<sup>5</sup> Moreover, with  $R_e = 6h^{-1}$  kpc, F15307-A would be somewhat small for a typical cD galaxy (Oegerle & Hoessel 1991). However, multiple merger events might occur in the formation history of all ellipticals, not just cD’s (Weil & Hernquist 1994). F15307-A itself may have formed at a higher redshift, and we are observing its subsequent interaction with components B and C at  $z = 0.93$ , whose outcome will be the consumption by component A of its two companions.

## 5. Conclusions

We have presented the highest spatial and spectral resolution near-IR observations to date of the  $\sim 10^{13} h^{-2} L_{\odot}$  *IRAS* galaxy FSC 15307+3252 located at  $z = 0.93$ , apparently the most luminous known galaxy. We find the following results:

1. Deep  $K$ -band images with  $0''.4$  resolution reveal at least three components to the system. The brightest, component A, is elliptical with a compact nucleus. Component B, is resolved and apparently circular, and the faintest component, C, has an irregular morphology.
2. The  $K$ -band surface brightness profile of F15307-A is well-described by a de Vaucouleurs  $r^{1/4}$  law with  $\mu_e = 20.1 \pm 0.3$  mag arcsec $^{-2}$  and  $r_e = 1''.4 \pm 0''.2$  ( $6h^{-1}$  kpc) after correction for

---

<sup>5</sup>The next most luminous *IRAS* galaxy after F15307, P09104+4109, with a luminosity of  $\sim 6 \times 10^{12} h^{-2} L_{\odot}$ , is a cD galaxy in a  $z = 0.44$  cluster (Kleinmann et al. 1988, Soifer et al. 1996).

seeing effects. Its effective radius is comparable to local giant ellipticals. After removal of the de Vaucouleurs profile, the core of F15307-A shows a compact nucleus with extended structure  $\sim 0''.5$  to the southwest, possibly a second nucleus.

3. Our 1.1–1.4  $\mu\text{m}$  (restframe optical) spectrum with a resolution of  $330 \text{ km s}^{-1}$  shows strong emission lines of [O I],  $\text{H}\alpha + [\text{N II}]$ , and [S II] with velocity widths typical of Seyfert 2 galaxies. The line excitation is also consistent with such a classification.  $\text{H}\alpha$  also has a strong  $\sim 1900 \text{ km s}^{-1}$  component but lacks a very broad  $\sim 10^4 \text{ km s}^{-1}$  component unlike the polarized Mg II  $\lambda 2798$  line (Cutri et al. 1994). The line emission may be extended on scales of  $\sim 1''$  ( $4h^{-1}$  kpc).

4. The morphology of F15307 is reminiscent of known gravitational lensed objects, particularly quadruply-imaged sources such as MG J0414+0534. Quantitative arguments are inconclusive, though if the system is lensed, the absence of an obvious foreground lens imply the lensing galaxy is underluminous for its mass. The fact that the components are extended means even if the system is lensed, the  $z = 0.93$  source must be an intrinsically luminous galaxy.

5. Alternatively, F15307 may be an interacting system with an intrinsically large luminosity, similar to local ultraluminous *IRAS* galaxies. Some indications exist that the system is not heavily extinguished. The  $r^{1/4}$  profile suggests F15037-A is an elliptical galaxy. It may be in the process of forming at  $z = 0.93$  or else it formed at  $z > 0.93$  and we are now observing its interaction/merger with components B and C.

Additional observations should determine the nature of F15307. *HST* imaging should be able to identify if the system is lensed but is not essential; ground-based IR observations in excellent seeing or high resolution radio imaging should also suffice. Color information will be useful — if the system is lensed, the foreground lensing galaxy, most likely an elliptical, should be distinct from the multiple images of the background lensed Seyfert. Narrow-band imaging centered on emission lines will be a good test for lensing as will long slit spectroscopy to compare the spectra of components A and B. One additional observation which would serve as an empirical test is to search for CO emission from F15307 since the only two definite detections of CO emission at high redshift are from the lensed sources F10214 and the Cloverleaf quasar (Solomon et al. 1992, Barvainis et al. 1994). Regardless of which way the issue is settled – if the system is a lensed Seyfert galaxy or an interacting elliptical — the system will be worthy of further scrutiny.

We are grateful to Tom Broadhurst, Luis Ho, Joe Shields, and Steve Zepf for useful discussions and thank Arjun Dey, George Djorgovski, and Hy Spinrad for their comments on a draft of this work. The W. M. Keck Observatory is a scientific partnership between the University of California and the California Institute of Technology, made possible by the generous gift of the W. M. Keck Foundation and support of its president, Howard Keck. It is a pleasure to thank Barbara Schaeffer, Wendy Harrison, and Imke de Pater for their help with these observations. J. R. G. is supported by a fellowship from the Packard Foundation and M. C. L. by an NSF Graduate Student Fellowship.

Table 1. Identification and Photometry of Sources in the F15307 Field

Object		$\Delta\alpha$ (")	$\Delta\delta$ (")	$K$ magnitude <sup>a</sup>
1		-19.2	13.3	$21.0 \pm 0.3$
2		-15.2	23.1	$22.5 \pm 1.0$
3		-14.4	20.4	$18.92 \pm 0.04$
4		-12.8	-9.2	$21.4 \pm 0.5$
5		-12.1	21.3	$22.8 \pm 1.1$
6		-11.7	25.9	$18.10 \pm 0.03$
7		-9.0	30.4	$17.81 \pm 0.03$
8		-8.3	7.5	$20.00 \pm 0.07$
9		-6.9	2.0	$20.37 \pm 0.10$
10		-3.2	-11.8	$18.85 \pm 0.02$
11		-2.0	10.6	$20.83 \pm 0.16$
12		-1.0	-7.5	$20.6 \pm 0.2$
13	F15307-A	0.0	0.0	$16.59 \pm 0.02$
14	F15307-B	1.4	-1.4	$18.40 \pm 0.02^b$
15	F15307-C	1.5	-0.2	$19.62 \pm 0.03^b$
16	bright star	2.8	19.5	$15.89 \pm 0.02$
17		4.6	-11.8	$19.54 \pm 0.10$
18		6.5	-9.4	$19.53 \pm 0.11$
19		8.4	26.8	$17.51 \pm 0.02$
20		9.6	-8.5	$19.8 \pm 0.2$
21		12.2	-1.0	$20.14 \pm 0.09$
22		13.3	23.0	$20.20 \pm 0.10$
23		13.5	14.1	$21.0 \pm 0.2$
24		14.5	8.6	$20.8 \pm 0.2$
25		17.5	6.6	$21.2 \pm 0.3$
26		17.9	-4.9	$18.93 \pm 0.06$
27		21.0	19.0	$20.4 \pm 0.2$
28		23.1	18.1	$20.2 \pm 0.2$
29		23.8	-6.6	$17.94 \pm 0.04$

<sup>a</sup>All photometry done in a 3" diameter aperture except for the components of F15307 which used 2" (component A), 1".5 (B), and 1" (C) diameter apertures. Values include a small aperture correction derived from the bright star. Errors were calculated by combining in quadrature the noise in the photometry aperture with errors in the zero point and sky level determination (§ 2.1).

<sup>b</sup>After removal of the best-fitting deVaucouleurs profile for component A, aperture-corrected photometry for components B and C gives  $18.6 \pm 0.1$  (1".5 diameter aperture) and  $20.1 \pm 0.3$  (1" aperture), respectively (§ 3.1.2).

Table 2. F15307 Emission Line Measurements

	$\lambda$ ( $\text{\AA}$ )	$z$	FWHM <sup>a</sup> ( $\text{km s}^{-1}$ )	Flux ( $10^{-19} \text{ W m}^{-2}$ )	Restframe equiv. width (nm)
[O I]	6300	$0.9288 \pm 0.0009$	$900 \pm 300$	$7 \pm 3$	$5 \pm 2$
	6364	$0.9288 \pm 0.0009$	$900 \pm 300$	$2.5 \pm 1.2$	$1.6 \pm 0.8$
[S II] <sup>b</sup>	6716	$0.9230 \pm 0.0014$	$900 \pm 600$	$2.2 \pm 1.8$	$1.5 \pm 1.3$
	6731	$0.9230 \pm 0.0014$	$900 \pm 600$	$5 \pm 4$	$3 \pm 3$
[N II] <sup>c</sup>	6548	$0.9280 \pm 0.0004$	$900 \pm 300$	$3.3 \pm 1.2$	$2.1 \pm 0.8$
	6583	$0.9280 \pm 0.0004$	$900 \pm 300$	$10 \pm 4$	$6 \pm 2$
H $\alpha$ (narrow) <sup>c</sup>	6563	$0.9280 \pm 0.0004$	$900 \pm 300$	$11 \pm 4$	$8 \pm 3$
(broad)	6563	$0.9280 \pm 0.0004$	$1910 \pm 50$	$39.4 \pm 1.3$	$25.8 \pm 0.9$

<sup>a</sup>uncorrected for instrumental broadening

<sup>b</sup>assumes high density limit for the ratio of the two lines

<sup>c</sup>FWHM fixed to be the same as [O I] (see § 3.2)

## REFERENCES

- Angonin-Willaime, M.-C., Vanderriest, C., Hammer, F., & Magain, P. 1994, *Å*, 281, 388
- Annis, J., & Luppino, G. A. 1993, *ApJ*, 407, L69
- Armus, L., Heckman, T. M., & Miley, G. K. 1990, *ApJ*, 364, 471
- Armus, L., Surace, J. A., Soifer, B. T., Matthews, K., Graham, J., & Larkin, J. E. 1994, *AJ*, 108, 76
- Barnes, J. E. 1992, *ApJ*, 393, 484
- Barnes, J. E., & Hernquist, L. E. 1992, *ARA&A*, 30, 705
- Barvainis, R., Tacconi, L., Antonucci, R., Alloin, D., & Coleman, P. 1994, *Nature*, 371, 586
- Beers, T. C., & Geller, M. J. 1983, *ApJ*, 274, 491
- Blandford, R. D., & Narayan, R. 1992, *ARA&A*, 30, 311
- Broadhurst, T. J., & Lehar, J. 1995, *ApJ*, 450, L41
- Bruzual A., G., & Charlot, S. 1993, *ApJ*, 405, 538
- Carico, D. P., Graham, J. R., Matthews, K., Wilson, T. D., Soifer, B. T., Neugebauer, G., & Sanders, D. B. 1990, *ApJ*, 349, L39
- Casali, M. M. & Hawarden, T. G. 1992, *JCMT-UKIRT Newsletter*, 4, 33
- Clowes, R. G., Campusano, L. E., Leggett, S. K., & Savage, A. 1995, *MNRAS*, 275, 819
- Condon, J. J. 1990, *ARA&A*, 30, 575
- Condon, J. J., Huang, Z.-P., Yin, Q. F., & Thuan, T. X. 1991, *ApJ*, 378, 65
- Cutri, R. M., Huchra, J. M., Low, F. J., Brown, R. L. & Vanden Bout, P. A. 1994, *ApJ*, 424, L65
- De Robertis, M. M., & Osterbrock, D. E. 1986, *ApJ*, 301, 727
- Djorgovski, S. & Davis, M. 1987, *ApJ*, 313, 59
- Djorgovski, S. et al. 1995, *ApJ*, 438, L13
- Doyon, R., Wells, M., Wright, G. S., Joseph, R. D., Nadeau, D., & James, P. A. 1994, *ApJ*, 437, L23
- Dunlop, J. S., Peacock, J. A., Savage, A., Lilly, S. J., Heasley, J. N., & Simon, A. J. B. 1989, *MNRAS*, 238, 1171

- Efstathiou, G. P., Ellis, R. S., & Peterson, B. A. 1988, MNRAS, 232, 431
- Eisenhardt, P. R., Armus, L., Hogg, D. W., Soifer, B. T., Neugebauer, G., & Werner, M. W. 1996, ApJ, 461, 72
- Elias, J. H., Frogel, J. A., Matthews, K., & Neugebauer, G. 1982, AJ, 87, 1029
- Faber, S. M., & Jackson, R. E. 1976, ApJ, 204, 668
- Fehmers, G. C., de Grijp, M. H. K., Miley, G. K., & Keel, W. C. 1995, A&AS, 108, 61
- Filippenko, A. 1985, ApJ, 289, 475
- Filippenko, A., & Halpern, J. 1984, ApJ, 285, 458
- Frogel, J. A., Persson, S. E., Aaronson, M., & Matthews, K. 1978, ApJ, 220, 75
- Gardner, J. P., Cowie, L. L., & Wainscoat, R. J. 1993, ApJ, 415, L9
- Garrett, M. A., Muxlow, T. W. B., Patnaik, A. R., & Walsh, D. 1994, MNRAS, 269, 902
- Gott, J. R., III 1977, ARA&A, 15, 235
- Gott, J. R., Park, M.-G., & Lee, H. M. 1989, ApJ, 338, 1
- Graham, J. R., Carico, D. P., Matthews, K., Neugebauer, G., Soifer, B. T., & Wilson, T. D. 1990, ApJ, 354, L5
- Graham, J. R., & Liu, M. C. 1995, ApJ, 449, L29
- Grossman, S. A., & Narayan, R. 1988, ApJ, 324, L37
- Hausman, M. A., & Ostriker, J. P. 1978, ApJ, 224, 320
- Hewitt, J.N., Turner, E. L., Lawrence, C. R., Schneider, D. P., & Brody, J. P. 1992, AJ, 104, 968
- Hines, D. C., Schmidt, G. D., Smith, P. S., Cutri, R. M., & Low, F. J. 1995, ApJ, 450, L1
- Ho, L. C., Filippenko, A. V., & Sargent, W. L. W. 1993, ApJ, 417, 63
- Ho, L. C., Shields, J. C., & Filippenko, A. V. 1993, ApJ, 410, 567
- Horne, K. 1986, PASP, 98, 609
- Kleinmann, S. G. et al. 1988, ApJ, 328, 161
- Kochanek, C. S. 1991, ApJ, 373, 354
- Kormendy, J., & Sanders, D. B. 1992, ApJ, 390, L53

- Kristian, J. et al. 1993, *ApJ*, 106, 1330
- Lake, G., & Dressler, A. 1986, *ApJ*, 310, 605
- Lawrence, C. R. et al. 1984, *Science*, 223, 46
- Leech, K. J., Rowan-Robinson, M., Lawrence, A., & Hughes, J. D. 1994, *MNRAS*, 267, 253
- Lucy, L. B. 1974, *AJ*, 79, 745
- Majewski, S. R., Hereld, M., Koo, D. C., Illingworth, G. D., & Heckman, T. M. 1993, *ApJ*, 402, 125
- Mathis, J. S. 1990, *ARA&A*, 28, 37
- Matthews, K. & Soifer, B. T. 1994, in *Infrared Astronomy with Arrays: The Next Generation*, ed. I. McLean (Dordrecht: Kluwer), 239
- Matthews, T. A., Morgan, W.W., & Schmidt, M. 1964, *ApJ*, 140, 35
- Melnick, J., & Mirabel, I. F. 1990, *A&A*, 231, L19
- Mihalas, D., & Binney, J. 1981, *Galactic Astronomy* (New York: W. H. Freeman and Co.)
- Morgan, W. W., Kayser, S., & White, R. A. 1975, *ApJ*, 199, 545
- Mountain C. M., Robertson, D. J., Lee, T. J., & Wade, R. 1990, in *Instrumentation in Astronomy VII*, ed. D. L. Crawford, *SPIE*, 1235, 25
- Oegerle, W. R., & Hoessel, J. G. 1991, *ApJ*, 375, 15
- Osterbrock, D. E. 1989, *Astrophysics of Gaseous Nebulae and Active Galactic Nuclei* (Mill Valley, CA: University Science Books)
- Osterbrock, D. E. 1991, *Rep. Prog. Phys.*, 54, 579
- Osterbrock, D. E., Shaw, R. A., & Veilleux, S. 1990, *ApJ*, 352, 561
- Pahre, M. A., Djorgovski, S. G., & de Carvalho, R. R. 1995, *ApJ*, 453, L17
- Peebles, P. J. E. 1993, *Principles of Physical Cosmology* (Princeton: Princeton University Press)
- Richardson, B. H. 1972, *Jour. Opt. Soc. Amer.*, 62, 55
- Rudy, R. J., Cohen, R. D., Rossano, G. S., Puetter, R. C., & Chapman, S. C. 1989, *ApJ*, 341, 120
- Rudy, R. J. et al. 1993, *ApJ*, 414, 527
- Sandage, A., & Perlmutter, J.-M. 1990, *ApJ*, 361, 1

- Sanders, D. B. 1992, in Relationships Between Active Galactic Nuclei and Starburst Galaxies, ed. Filippenko, A. V., Astr. Soc. of Pacific. Conf. Ser., 31, 303
- Sanders, D. B., Soifer, B. T., Elias, J. H., Madore, B. F., Matthews, K., Neugebauer, G., & Scoville, N. Z. 1988a, ApJ, 325, 74
- Sanders, D. B., Soifer, B. T., Elias, J. H., Neugebauer, G., & Matthews, K. 1988b, ApJ, 328, L35
- Schneider, D. P., Gunn, J. E., Turner, E. L., Lawrence, C. R., Hewitt, J. N., Schmidt, M., & Burke, B. 1986, AJ, 91, 991
- Schweizer, F. 1982, ApJ, 252, 455
- Shortridge, K. 1993, in Astronomical Data Analysis Software and Systems II, ASP Conf. Ser., 52, 219
- Soifer, B. T., Neugebauer, G., Armus, L., & Shupe, D. L. 1996, AJ, in press
- Soifer, B. T., Neugebauer, G., Matthews, K., & Armus, L. 1994, ApJ, 433, L69
- Soifer, B. T., Sanders, D. B., Neugebauer, G., Danielson, G. E., Lonsdale, C. J., Madore, B. F., & Persson, S. E. 1986, ApJ, 303, L41
- Solomon, P. M., Radford, S. J. E., & Downes, D. 1992, Nature, 356, 318
- Stanford, S. A., & Bushouse, H. A. 1991, ApJ, 371, 92
- Tadhunter, C. N. et al. 1988, MNRAS, 235, 403
- Toomre, A., & Toomre, J. 1972, ApJ, 178, 623
- Trentham, N. 1995, MNRAS, 277, 616
- Turner, E. L., Ostriker, J. P., & Gott, J. R., III. 1984, ApJ, 284, 1
- Veilleux, S., Kim, D.-C., Sanders, D. B., Mazzarella, J. M., & Soifer, B. T. 1995, ApJS, 98, 171
- Veilleux, S., & Osterbrock, D. E. 1987, ApJS, 63, 295
- Weil, M. L., & Hernquist, L. 1994, ApJ, 431, L79
- Weymann, R. J. et al. 1980, Nature, 285, 641
- Woltjer, L. 1990, in Active Galactic Nuclei: Saas-Fee Advanced Course 20 Lecture Notes, ed. Courvoisier, T. J.-L. & Mayor, M. (Berlin: Springer-Verlag), 1
- Wright, G. S., James, P. A., Joseph, R. D., & McLean, I. S. 1990, Nature, 344, 417
- Young, P., Deverill, R. S., Gunn, J. E. & Westphal, J. A. 1981, ApJ, 244, 723

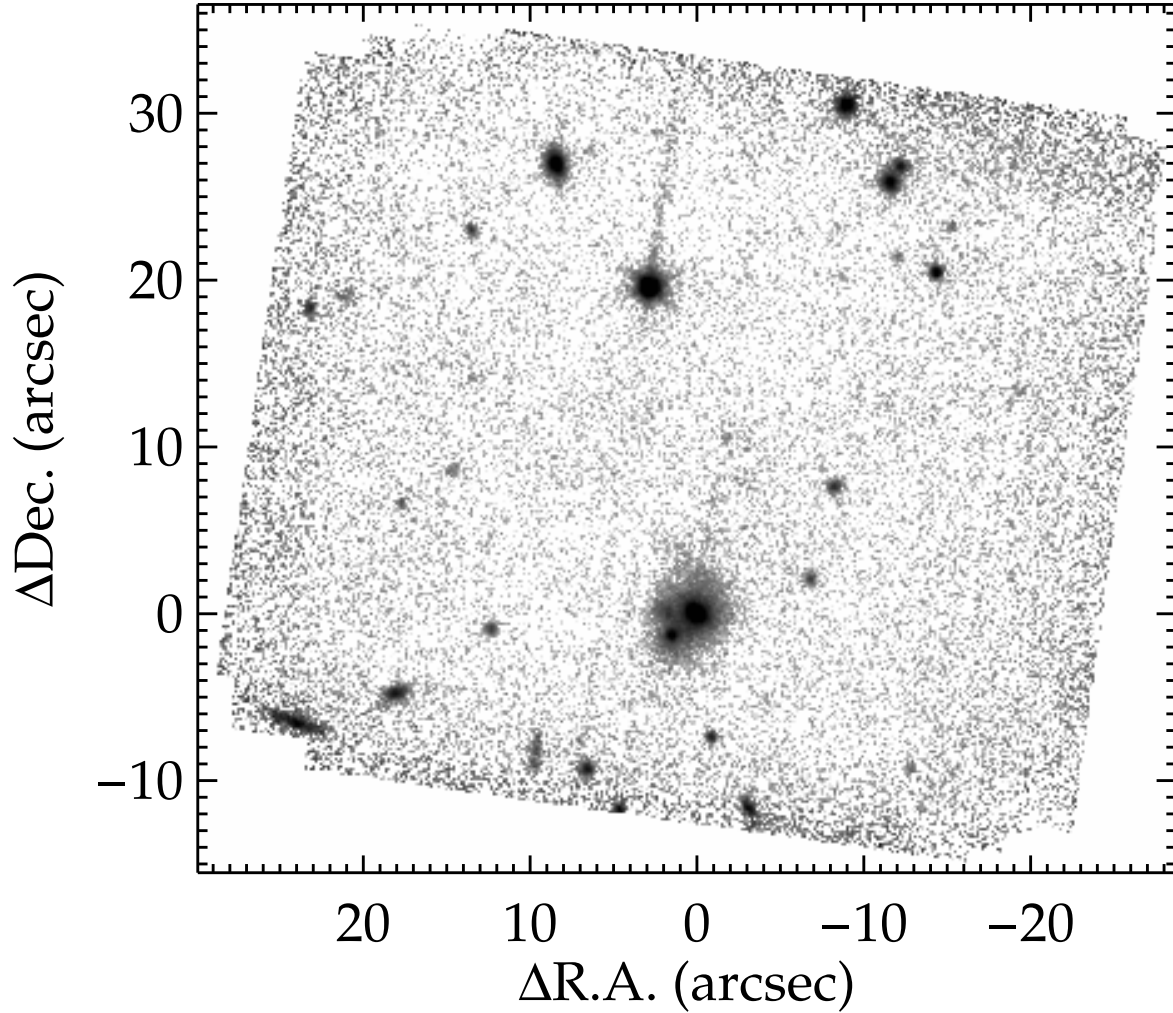


Fig. 1.—  $K$ -band mosaic of the F15307 field obtained in  $0''.4$  seeing at the W. M. Keck Telescope. North is up and east to the left. The greyscale is logarithmic. F15307 is the large galaxy with multiple components at the origin of the axes. The deepest portion of the mosaic achieves  $1\sigma$  noise of  $23.9 \text{ mag arcsec}^{-2}$ , and the faintest objects are  $K \approx 21.5 - 22$ . The long northern tail of the brightest star in the field is an artifact of the data acquisition and is not physically significant. For our assumed cosmology ( $q_0 = 0.5$ ,  $H_0 = 100h \text{ km s}^{-1} \text{ Mpc}^{-1}$ ),  $1''$  corresponds to  $4.2h^{-1} \text{ kpc}$ .

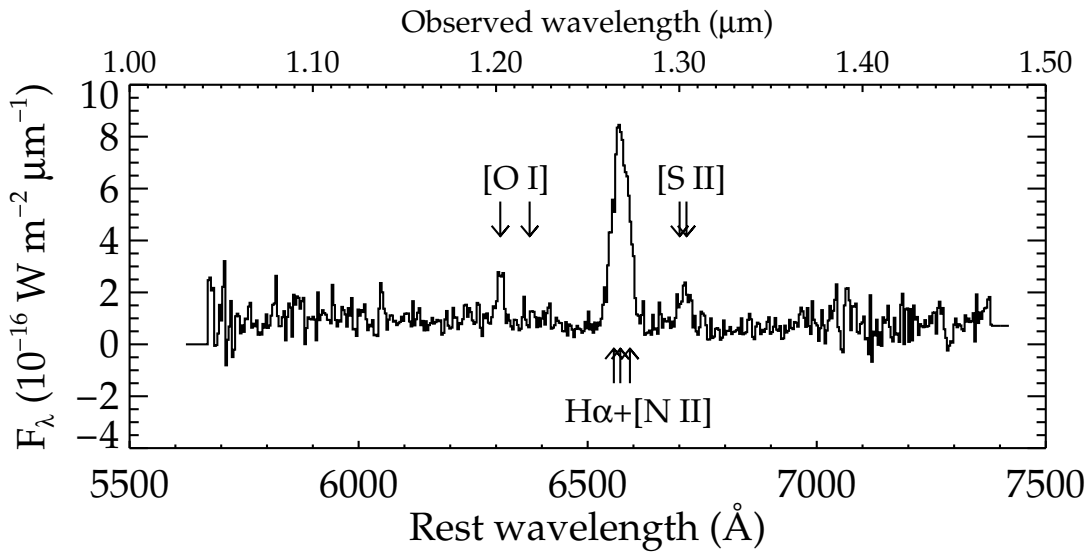


Fig. 2.— *J*-band spectrum of F15307. Emission lines of [O I]  $\lambda\lambda 6300, 6364$ ; blended H $\alpha$  + [N II]  $\lambda\lambda 6548, 6583$ ; and [S II]  $\lambda\lambda 6716, 6731$  are observed and spectrally resolved. The resolution is  $330 \text{ km s}^{-1}$  (2 pixels). The rest wavelength scale assumes a redshift of 0.926.

# IRAS FSC 15307+3252

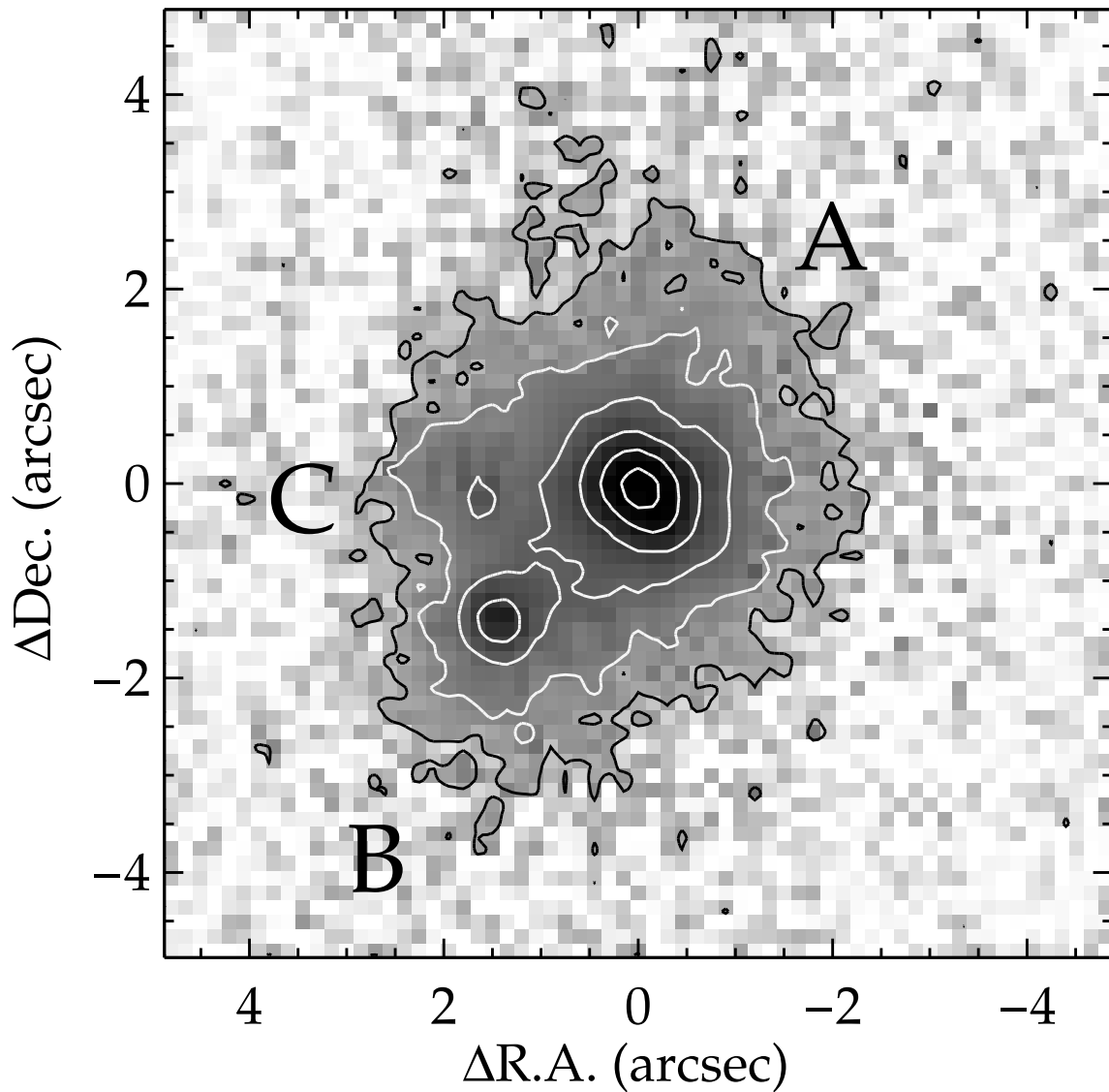


Fig. 3.— A close view of the  $K$ -band image of F15307 along with the designations we assign to the separate components based on their relative  $K$  magnitudes (§ 3.1). Again, the greyscale is logarithmic. All three components are extended. Contours are spaced by 1 magnitude (factor 2.5) with the brightest contour being  $16.3 \text{ mag arcsec}^{-2}$ . For our assumed cosmology ( $q_0 = 0.5$ ,  $H_0 = 100h \text{ km s}^{-1} \text{ Mpc}^{-1}$ ),  $1''$  corresponds to  $4.2h^{-1} \text{ kpc}$ .

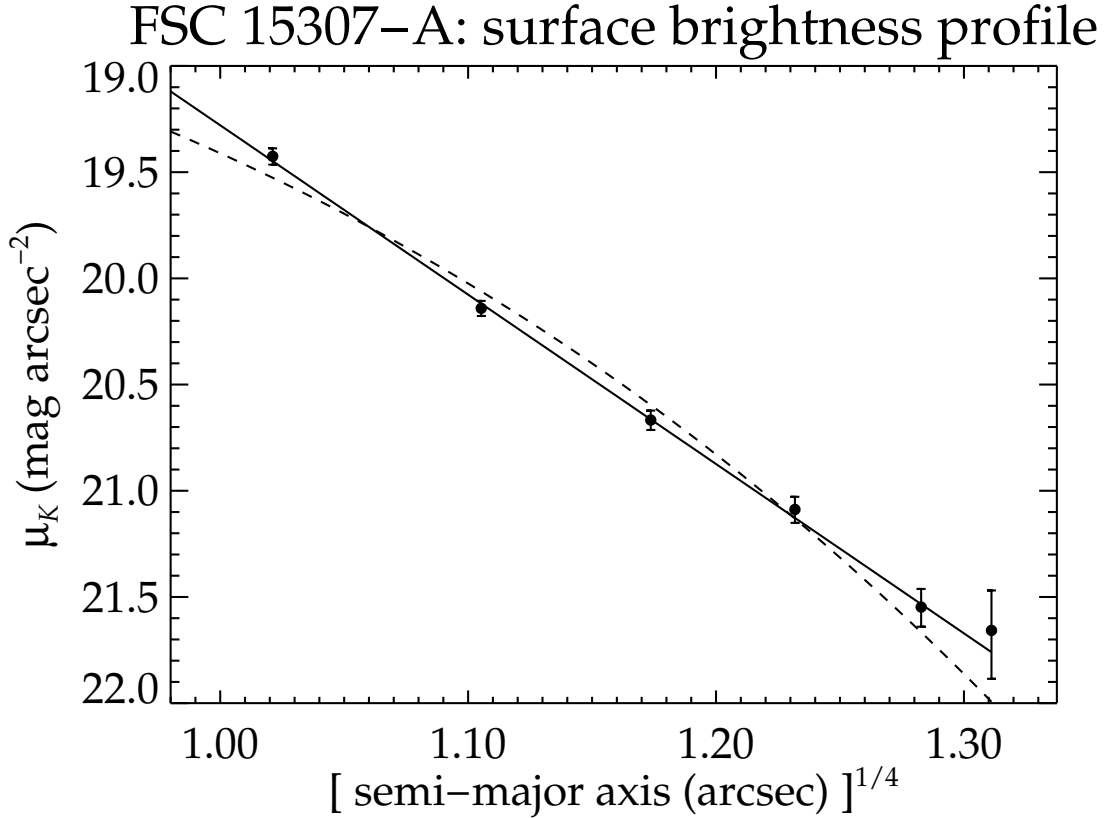


Fig. 4.— A plot of the surface brightness profile of component A, extracted using elliptical apertures of a fixed position angle and axial ratio spaced by the  $0''.4$  seeing FWHM (§ 3.1.1). The solid line shows a de Vaucouleurs profile fitted from  $1''$ – $3''$  ( $\tilde{\chi}^2 = 0.4$ ), and the dashed line is an exponential disk fit ( $\tilde{\chi}^2 = 4.7$ ) — clearly the de Vaucouleurs fit is superior. After correcting for systematic effects due to seeing, we find  $\mu_e = 20.1 \pm 0.3$  mag arcsec<sup>-2</sup> and  $r_e = 1''.4 \pm 0''.2$  ( $6h^{-1}$  kpc for  $H_0 = 100h$  km s<sup>-1</sup> Mpc<sup>-1</sup> and  $q_0 = 0.5$ ), a size comparable to local giant elliptical galaxies (§ 4.2).

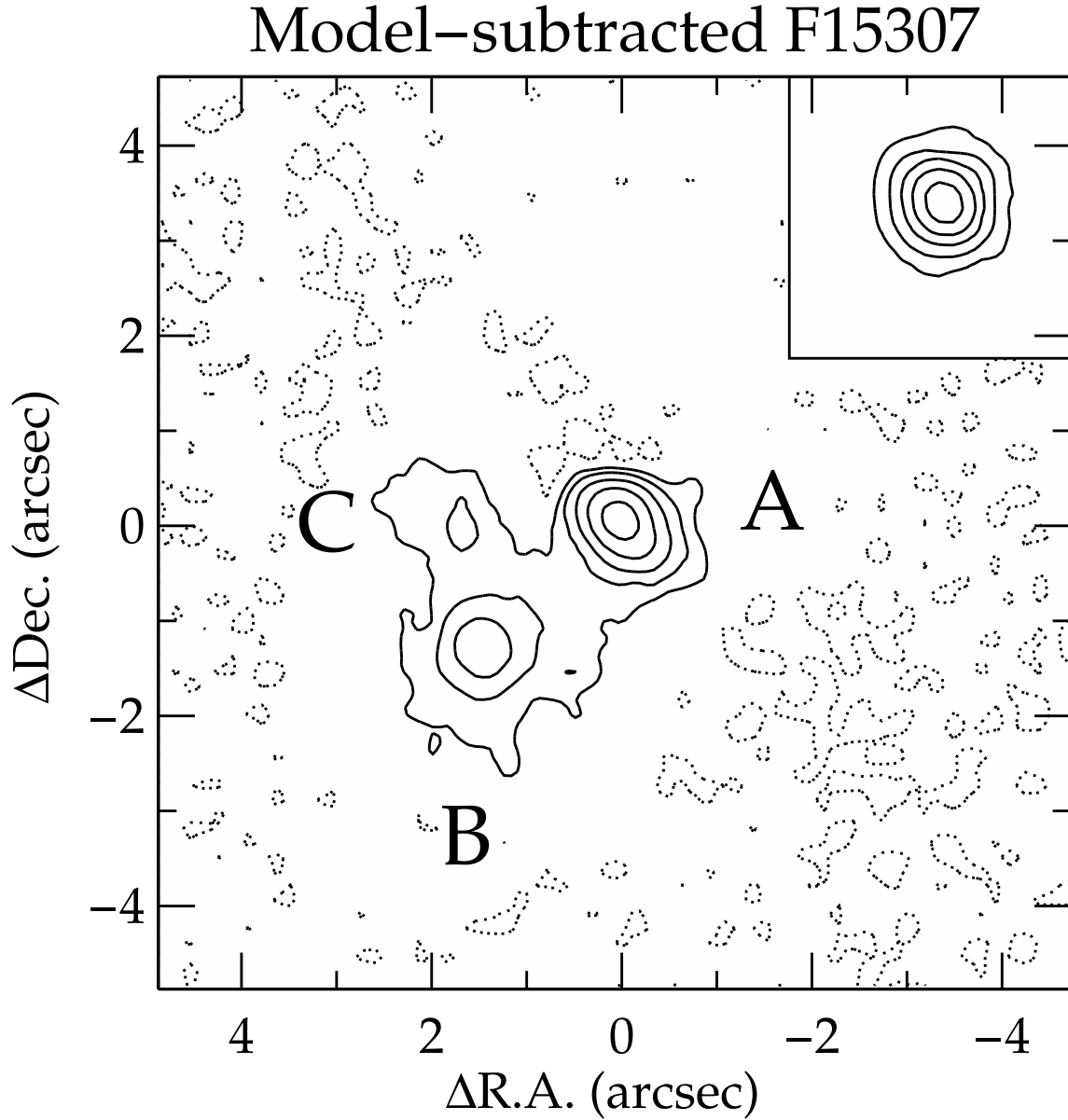


Fig. 5.— *K*-band image of F15307 after removal of the best-fitting de Vaucouleurs profile centered on component A (§3.1.1). The inset shows the point spread function as measured by the bright star in the field for comparison. The contours for both images start at 64% of the peak value and decrease by factors of 2.5. The dotted contours represent  $-1\%$  of the peak. The residuals at the center of component A show an unresolved source with an extension or second nucleus  $\sim 0''.5$  to the southwest. Components B and C are clearly seen as is a bridge of emission between A and B.